

The Anomalous Resonant Frequency Variation of Microwave Superconducting Niobium Cavities Near T_c

D. Bafia,^{1,*} A. Grassellino,¹ M. Checchin,¹ J. F. Zasadzinski,² and A. Romanenko¹

¹*Fermi National Accelerator Laboratory, Batavia, Illinois 60510, USA*

²*Department of Physics, Illinois Institute of Technology, Chicago, Illinois 60616, USA*

(Dated: January 6, 2022)

Superconducting radio-frequency (SRF) niobium cavities are the modern means of particle acceleration and an enabling technology for record coherence superconducting quantum systems and ultra-sensitive searches for new physics. Here, we report a systematic effect in Nb cavities indicative of improved superconducting properties - an anomalous decrease (dip) in the resonant frequency at temperatures just below the critical temperature T_c . The frequency dip magnitude correlates with cavity quality factor, near-surface impurity distribution, and T_c . It is also a precursor of the peculiar decrease in the BCS surface impedance with increasing RF current. A first demonstration of the coherence peak in the AC conductivity in Nb SRF cavities is also presented and found to correlate with a large frequency dip.

Superconducting radio-frequency (SRF) niobium cavities are record-high quality factor $Q_0 > 10^{10} - 10^{11}$ man-made resonators that serve as the primary continuous wave accelerating structures in modern particle accelerators [1], longest coherence microwave quantum superconducting systems [2], and an ultra-sensitive platform for dark sector and dark matter candidate searches [3–6].

An important feature of SRF cavities is the commonly observed reduction of the Q_0 (Q-slope) with the magnitude of the stored microwave field. Extensive research over the past decades allowed uncovering and mitigating several such field-dependent physical mechanisms in various regimes [1]. This most recently includes proximity-coupled niobium nanohydrides [7] and their mitigation by oxygen inward diffusion [8] and the reduction of two-level system driven dissipation by oxide removal [2, 9].

This steady improvement has unveiled new SRF phenomena that remain poorly understood, most notably the factor of four increase in Q_0 and the field-dependent *increase* in the quality factor of nitrogen doped [10] cavities. A comparison to more standard surface treatments such as electropolishing (EP) is shown in Fig. 1. The unusual effect, often called the anti-Q slope (top curve of Fig. 1), stems from an anomalous decrease of the “BCS” component [11] of the surface resistance with increasing field [10]. This effect challenges our understanding; in essence, it is as if superconducting pairing strengthens with increased RF field and current, an effect that is counterintuitive. Material studies have highlighted its dependence on the near-surface interstitial nitrogen concentration and distribution. For the microscopic mechanism, one suggested possibility is the field-driven non-equilibrium redistribution of thermally excited quasiparticles to higher energy levels. Studies on cavities of different frequencies [12] provide support for this possibility. Still, a systematic study of the effect of doping on quasiparticle lifetimes and density of states as well as strong coupling pairing effects in SRF cavities has not been reported and is critical for the understanding of the effect.

While many studies have focused on the quality factor, here we report that the cavity resonant frequency provides another valuable avenue for gaining insight into the underlying physical phenomena, as its changes are directly connected to the properties of the superconducting condensate. The inset of Fig. 1 shows a correlation of cavity Q_0 at a field strength of 16 MV/m with the magnitude of an anomalous frequency drop observed just below the critical transition temperature T_c . Detailed examination of this unusual frequency drop is presented here.

The AC complex conductivity $\sigma = \sigma_1 + i\sigma_2$ enables further insight on quasiparticles and superconducting carriers. For frequencies far below the superconducting gap ($\hbar\omega \ll \Delta$), σ_1 exhibits the coherence peak, a non-monotonic dependence of the quasiparticle conductivity with temperature that arises due to coherence factors in BCS theory [13] and is analogous to the Hebel-Slichter peak in nuclear spin relaxation [14]. However, until now, this coherence peak has not been reported in Nb SRF cavities. It will be shown that the height of the coherence peak also correlates with the frequency drop. Taken together, these correlated phenomena suggest that extrinsic factors have prevented the observation of novel intrinsic RF properties of strong-coupled Nb. We comment later on possible origins for the correlations among these unusual observations.

In this article, a systematic study is presented on a large number (>40) of state-of-the-art bulk niobium SRF cavities revealing the anomalous decrease (dip) in the cavity resonant frequency at temperatures just below T_c in nitrogen doped cavities. In addition, we report other (non-dip) characteristic temperature dependencies uniquely corresponding to each of the other explored surface treatments that show strong correlation with cavity performance and the anti-Q slope. The measured coherence peak in the complex conductivity of bulk niobium SRF cavities is fit with a phenomenological model incorporating a pair-breaking term in the BCS density of states. The fits suggest that the coherence peak, along

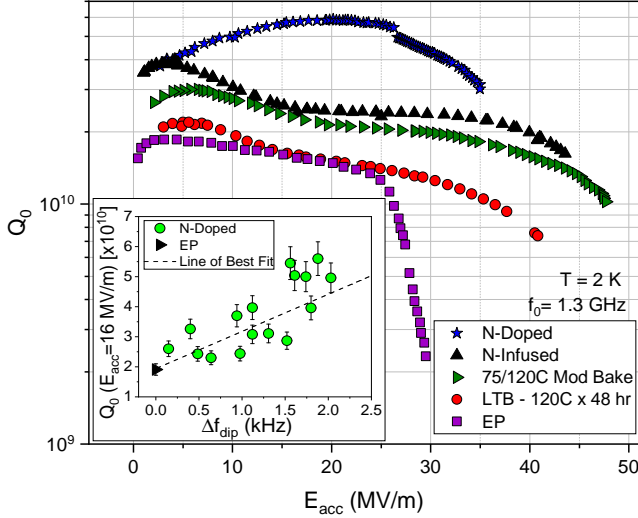


FIG. 1. CW RF test results of Nb SRF cavities subjected to surface treatments used in this study. Inset plots Q_0 at 16 MV/m at 2 K against the measured dip magnitude of cavities subjected to either EP or various N-doping surface treatments.

with the dip phenomenon, high Q_0 , and anti-Q slope, are signatures of improved superconducting properties and occur when extrinsic pair-breaking effects are minimized. Furthermore, an understanding of the frequency dip may be a key to the microscopic origin of the anti-Q slope.

A large set of bulk niobium SRF cavities of TESLA [15] elliptical shape were employed for our studies. The resonant frequencies of these cavities varied from 650 MHz to 3.9 GHz, which allowed probing the low frequency limit of Nb. All cavities went through a bulk electropolishing of 120 μm material removal followed by different modern surface treatments on subsets of multiple cavities in each. The treatments investigated included hydrogen degassing at 800°C followed by additional 40 μm electropolishing, nitrogen doping [10] with varying dopant concentrations, nitrogen infusion [16], 120°C baking for 48 hours [17], and “modified” 75/120°C baking [18, 19]. One of the nitrogen doped cavities has been studied with a step-by-step material removal after initial doping to directly probe the effect of gradual changes in interstitial nitrogen concentration on cavity performance.

All cavities were first cooled down to 2 K where standard measurements [20] of Q_0 as a function of the accelerating gradient E_{acc} have been performed. Characteristic $Q_0(E_{\text{acc}})$ curves are shown in Fig. 1.

Measurements of the resonant frequency f_0 with temperature were performed as follows. All cavities were equipped with resistance temperature detectors (RTDs), placed in a helium dewar, and pre-cooled to 4.2 K. Heaters located at the bottom were used to boil off the liquid helium and warm the dewar. This procedure allowed for a warming rate of < 0.1 K/min, ensuring ther-

malization of the cavity, as confirmed by the RTD readings. Resonant frequency was recorded with a vector network analyzer. Measurements persisted through the niobium superconducting transition temperature at ~ 9.2 K. After measurements, the data was corrected to account for variations in dewar gas pressure.

For each $f_0(T)$ dataset, an effective mean free path ℓ within the cavity surface layer has been obtained by converting the measured frequency shift with temperature near T_c into a shift in the magnetic field penetration depth $\lambda(T)$ using Slater’s theorem [21] and fitting based on the modified Halbritter routine [22], following the same technique outlined in [23].

Overall, we have studied the frequency response of 41 cavities with various impurity structures in the RF layer. Of these 41, we found a clear dip in the resonant frequency just below the T_c in 22 N-doped cavities, similar to the one shown in Fig. 2(b). For other treatments, we observed four other characteristic behaviors, which we labeled “foot”, “bump”, “dip+bump”, and “standard.” More details are provided in the Supplemental Material.

To investigate the dependence of the dip on the nitrogen concentration, one cavity subjected to 3/60 nitrogen doping underwent several sequential material removal steps of the RF surface *via* EP, with RF measurements performed after each step. The material removal allowed to gradually decrease the concentration of N present in the RF layer, resulting in an increase in ℓ . After the combined 30 μm material removal, the cavity was bulk electropolished and re-processed with the 2/6 N-doping surface treatment. The $Q_0(E_{\text{acc}})$ and $f_0(T)$ results along with the corresponding material removal amounts and extracted ℓ values are presented in Fig. 2.

We observe that dilute and uniform concentrations of nitrogen (short ℓ) produce a characteristic increase in Q_0 at higher E_{acc} , a weak suppression in T_c , and an anomalous frequency dip just before T_c . As nitrogen concentration gradually decreases with more material removal, these behaviors are gradually diminished. The Q_0 behavior with field approaches that of the typical EP cavity presented in Fig. 1. Meanwhile, the dip magnitude diminishes as the transition temperature assumes the clean niobium value. Subsequent bulk electropolishing and 2/6 doping, which is known to produce a larger nitrogen concentration than 3/60 doping, shows a return of the dip feature with a larger magnitude and lower T_c .

Fig. 2(c) plots the dip magnitude and transition temperature against ℓ . The dip magnitude decreases strongly (close to exponentially) while the transition temperature increases with increasing ℓ values. The T_c varies by ~ 120 mK throughout the course of the study, which is in good agreement with previous work on the effects of nitrogen and oxygen on niobium T_c [24]. Our findings clearly show that a frequency dip and corresponding T_c suppression occur in the presence of uniform and dilute concentrations of N impurities and that the concentra-

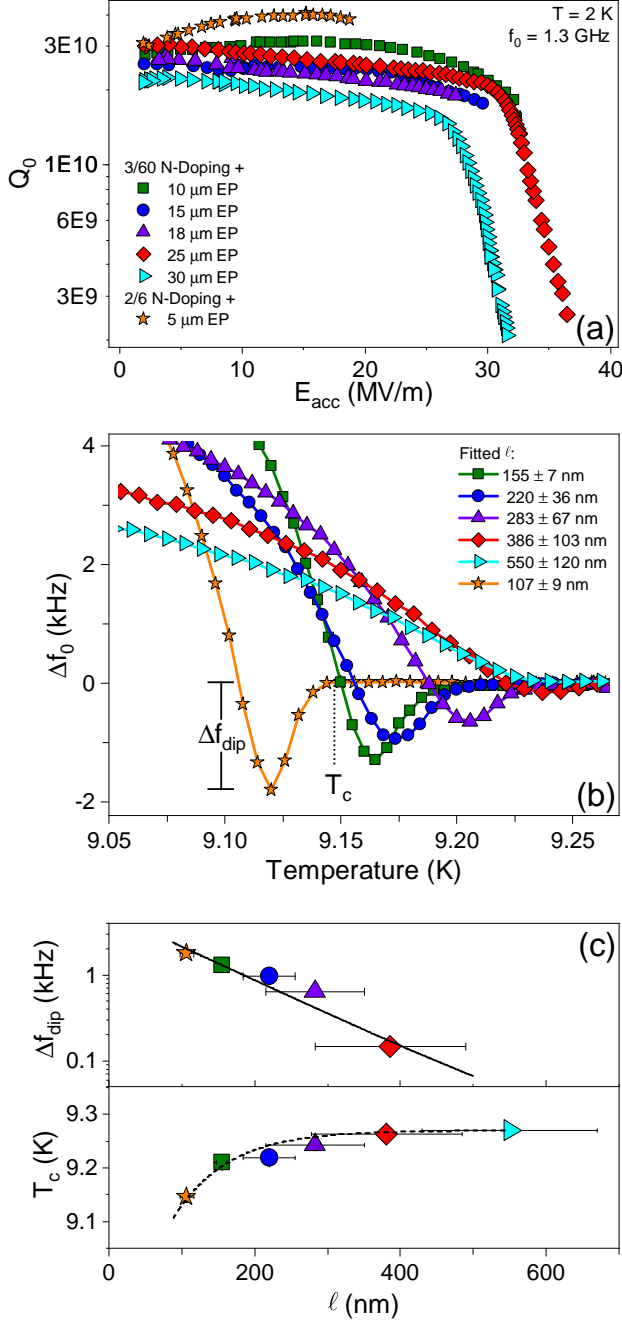


FIG. 2. (a) CW RF measurements and (b) resonant frequency response with temperature of a single 1.3 GHz Nb cavity after sequential removal of the surface post nitrogen doping. The legend in (b) presents the fitted ℓ in the RF layer after each step. Resonant frequency shift is reported relative to the normal conducting value near 10 K. The parameter Δf_{dip} is called the dip magnitude and T_c is the critical transition temperature. (c) The dip magnitude and T_c are plotted against the fitted ℓ . Horizontal error bars come from fitting while vertical error bars are smaller than the data points. Solid and dashed lines show $e^{-\ell}$ and $-e^{-\ell}$ relationships, respectively.

tion of N serves as a major parameter in determining the

extent of the phenomena.

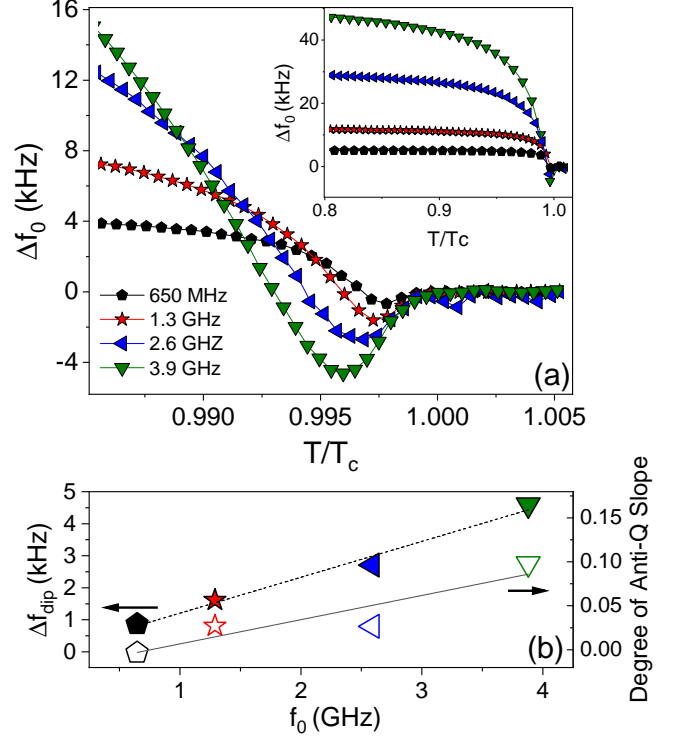


FIG. 3. (a) Frequency response with temperature of four cavities, each with different resonant frequency, processed to yield an identical nitrogen concentration in the RF layer. Inset shows the response over a larger range of temperatures. (b) Left-hand axis shows the dip magnitude plotted against the fundamental resonant frequency for each cavity. The right-hand axis plots the degree of anti-Q slope of each cavity, as defined in the text. Dashed and solid lines show linear fits.

To study the effect of resonant frequency on the dip, four niobium cavities with $f_0 = 650$ MHz, 1.3 GHz, 2.6 GHz, and 3.9 GHz were subjected to the same N-doping surface treatment, producing an identical impurity structure in each cavity. The results are shown in Fig. 3(a). We observe that resonant frequency is linearly related with the dip magnitude, as shown in Fig. 3(b). Furthermore, the degree of anti-Q slope, defined here as the slope from 2 MV/m to 15 MV/m of the $Q_0(E_{acc})$ curve normalized to the value at 2 MV/m, also exhibits a linear trend with the resonant frequency. A similar dependence of the anti-Q slope is shown in [12] where it is hypothesized that such behavior may be driven by non-equilibrium superconductivity. This correlation suggests that the frequency dip is a fundamental property that is directly related to the anti-Q slope phenomenon of N-doped cavities.

To gain insight on the conditions under which different frequency features near T_c occur, we measured the AC complex conductivity of two niobium cavities: i) the cavity presented in Fig. 2(a) with $\ell = 550 \pm 120$ nm which showed the standard feature near T_c and ii) a nitro-

gen doped cavity that exhibited the prominent dip. The transition temperature of the latter cavity was 9.04 K; using Fig. 2(c), the extrapolated ℓ was about 70 nm. Normalized values of σ_1 and σ_2 have been obtained from $Q_0(T)$ and $f_0(T)$ data using the method discussed by Trunin [25]. We accounted for anomalous skin effects by using theory from Reuter and Sondheimer [26]. This method required the measurement of the surface impedance for $2 < T < 10$ K using the methods laid out in [27]. The calculated conductivities are presented in Fig. 4. As the technique used to measure the surface impedance sums over the inner surface, these curves represent the average cavity response. Details on the technique are given in the Supplemental Material.

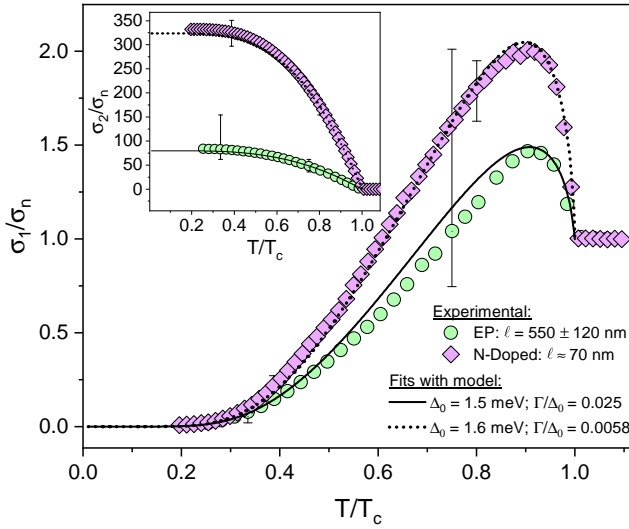


FIG. 4. Real and imaginary parts of the AC conductivity normalized to the normal conducting value σ_n of two 1.3 GHz cavities treated with EP or N-doping. Error bars for the test post N-doping are dominated by measurement uncertainty while those shown post EP are dominated by error in the fitted ℓ value. Dashed and solid lines show fits.

From Fig. 4, we observe that both the EP and N-doped cavities exhibit the so-called coherence peak, with the maxima at $\sim 0.9 T/T_c$ differing in amplitude. This suggests a variation in the quasiparticle behavior within the RF layer due to distinct impurity distributions.

The dashed and solid curves in Fig. 4 are calculated using a modified version of the Mattis-Bardeen (MB) conductivity with the Dynes inelastic scattering, or depairing rate parameter Γ [28] built in. This phenomenological model, which is further discussed in the Supplemental Materials, gives a measure of pair-breaking in the RF surface by introducing subgap quasiparticle states and reproduces some of the salient features discussed in more rigorous theories at low Γ/Δ_0 values [29–31].

We find that both σ_1 and σ_2 of the EP cavity are best modelled with an average superconducting gap $\Delta_0 = 1.5$ meV and an inelastic scattering parameter

$\Gamma/\Delta_0 = 0.025$. The N-doped cavity is instead better fitted with a larger average superconducting gap $\Delta_0 = 1.6$ meV and a lower level of pair-breaking ($\Gamma/\Delta_0 = 0.0058$). Recent work by Herman [32] has fitted this conductivity data with an alternative theory that also considers the Dynes parameter. The fits produced in that work are in qualitative agreement with the observations made using the present phenomenological model. Notice that the stronger coherence peak occurs for the cavity with the shorter ℓ . This follows Anderson’s theorem in that elastic scattering has no effect on superconductivity. But higher elastic scattering is indicative of N interstitials that are mitigating depairing processes.

These values are consistent with point contact tunneling spectroscopy (PCTS) studies by Groll *et al.* on similarly treated cavity cutouts [33]. The N-doped samples in those studies show more homogeneous Δ_0 values and lower levels of Γ/Δ_0 than those that come from EP cavities [34]. This gives one possible cause for the difference in gap values obtained from the fits shown in Fig. 4; electropolished cavities contain localized defective regions that bring down the average superconducting gap. The lower level of pair-breaking observed in Fig. 4 for the N-doped cavity is likely due to the absence (or lower volume fraction) of proximity coupled nanohydrides and magnetic moments within the interface. This is consistent with the fact that N-doped cavities do not exhibit the high field Q drop caused by the proximity breakdown of hydrides at high fields [7, 10].

These observations imply that superconducting niobium which contains a minimal level of depairing processes in the RF layer exhibits both the anti- Q slope and the frequency dip.

While a full microscopic model for the frequency dip has not yet been realized, there remain several candidates. One possibility is current redistribution which may cause an increase in the surface impedance [35]. Another alternative is that the phenomenon stems directly from MB theory [36]. Additionally, the AC susceptibility has been shown to exhibit similar phenomena near T_c that lead to the paramagnetic Meissner effect [37] or when considering anisotropic effects in the AC response of the Meissner state [38].

Although we focus primarily on the “dip” and “standard” features, it is likely that the three other frequency features near T_c follow some relationship with ℓ , Γ/Δ_0 , and Δ_0 as well. This will be a topic of future study.

In summary, we have presented systematic studies of an anomalous resonant frequency behavior near T_c of bulk niobium SRF cavities that correlates directly with $Q_0(E_{acc})$ and the novel anti- Q -slope state. Thus, an understanding of the frequency dip may shed new light on details of the surface superconductivity. Furthermore, the first observation of the coherence peak in these structures was presented and it was shown that the strength of this peak correlates with reduced pairbreaking in the sur-

face layer. This latter effect implies that a dilute concentration of N interstitials prevents the formation of surface irregularities (e.g. hydrides, magnetic oxides) that cause depairing, allowing intrinsic properties to be revealed. These findings open a new avenue for understanding the underlying fundamental physics behind the increase of the SRF cavity Q_0 with field in nitrogen doped cavities. In particular, the proposed non-equilibrium redistribution of quasiparticle states may rely on the low inelastic scattering (or recombination) rates measured here. Thus, while the high Q_0 values of these N-doped cavities are of technological interest for a host of accelerator applications, it may also be pointing to novel superconductivity in Nb under these intense fields of microwave photons.

The authors would like to acknowledge O. Melnychuk and D. A. Sergatskov for technical support during measurements. Work supported by the Fermi National Accelerator Laboratory, managed and operated by Fermi Research Alliance, LLC under Contract No. DE-AC02-07CH11359 with the U.S. Department of Energy.

* dbafia@fnal.gov

- [1] H. S. Padamsee, Annu. Rev. Nucl. Part. Sci. **64**, 175 (2014).
- [2] A. Romanenko, R. Pilipenko, S. Zorzetti, D. Frolov, M. Awida, S. Belomestnykh, S. Posen, and A. Grassellino, Phys. Rev. Appl. **13**, 034032 (2020).
- [3] R. Janish, V. Narayan, S. Rajendran, and P. Riggins, Phys. Rev. D **100**, 015036 (2019).
- [4] Z. Bogorad, A. Hook, Y. Kahn, and Y. Soreq, Phys. Rev. Lett. **123**, 021801 (2019).
- [5] A. Berlin, R. T. D'Agnolo, S. A. R. Ellis, C. Nantista, J. Neilson, P. Schuster, S. Tantawi, N. Toro, and K. Zhou, J. High Energy Phys. **2020**, 88 (2020).
- [6] C. Gao and R. Harnik, ArXiv:2011.01350.
- [7] A. Romanenko, F. Barkov, L. D. Cooley, and A. Grassellino, Supercond. Sci. and Technol. **26**, 035003 (2013).
- [8] A. Romanenko, Y. Trenikhina, M. Martinello, D. Bafia, and A. Grassellino, in *Proceedings of the 19th International Conference on RF Superconductivity* (HZDR, Dresden, Germany, 2019) p. 866.
- [9] A. Romanenko and D. I. Schuster, Phys. Rev. Lett. **119**, 264801 (2017).
- [10] A. Grassellino, A. Romanenko, D. Sergatskov, O. Melnychuk, Y. Trenikhina, A. Crawford, A. Rowe, M. Wong, T. Khabiboulline, and F. Barkov, Supercond. Sci. and Technol. **26**, 102001 (2013).
- [11] D. C. Mattis and J. Bardeen, Phys. Rev. **111**, 412 (1958).
- [12] M. Martinello, M. Checchin, A. Romanenko, A. Grassellino, S. Aderhold, S. K. Chandrasekaran, O. Melnychuk, S. Posen, and D. A. Sergatskov, Phys. Rev. Lett. **121**, 224801 (2018).
- [13] J. Bardeen, L. N. Cooper, and J. R. Schrieffer, Phys. Rev. **108**, 1175 (1957).
- [14] L. C. Hebel and C. P. Slichter, Phys. Rev. **113**, 1504 (1959).
- [15] B. Aune *et al.*, Phys. Rev. ST Accel. Beams **3**, 092001 (2000).
- [16] A. Grassellino, A. Romanenko, Y. Trenikhina, M. Checchin, M. Martinello, O. S. Melnychuk, S. Chandrasekaran, D. A. Sergatskov, S. Posen, A. C. Crawford, S. Aderhold, and D. Bice, Supercond. Sci. Technol. **30**, 094004 (2017).
- [17] H. Padamsee, *RF Superconductivity: Volume II: Science, Technology and Applications* (Wiley-VCH Verlag GmbH and Co., KGaA, Weinheim, 2009).
- [18] A. Grassellino, A. Romanenko, D. Bice, O. Melnychuk, A. C. Crawford, S. Chandrasekaran, Z. Sung, D. A. Sergatskov, M. Checchin, S. Posen, M. Martinello, and G. Wu, ArXiv:1806.09824.
- [19] D. Bafia, A. Grassellino, O. Melnychuk, A. Romanenko, Z.-H. Sung, and J. Zasadzinski, in *Proceedings of the 19th International Conference on RF Superconductivity* (HZDR, Dresden, Germany, 2019) p. 586.
- [20] O. Melnychuk, A. Grassellino, and A. Romanenko, Rev. Sci. Instrum. **85**, 124705 (2014).
- [21] J. C. Slater, Rev. Mod. Phys. **18**, 441 (1946).
- [22] J. Halbritter, Institut für Experimentelle Kernphysik (IEKP), Report No. KFK-Extern 03/70-06 (1970).
- [23] M. Martinello, A. Grassellino, M. Checchin, A. Romanenko, O. Melnychuk, D. A. Sergatskov, S. Posen, and J. F. Zasadzinski, Appl. Phys. Lett. **109**, 062601 (2016).
- [24] W. DeSorbo, Phys. Rev. **132**, 107 (1963).
- [25] M. R. Trunin, A. A. Zhukov, and A. T. Sokolov, Zh. Eksp. Teor. Fiz. **111**, 696 (1997).
- [26] G. E. H. Reuter and E. H. Sondheimer, Proc. Roy. Soc. London Ser. A **195**, 336 (1948).
- [27] D. Bafia, Ph.D. thesis, Illinois Institute of Technology (2020).
- [28] R. C. Dynes, V. Narayanamurti, and J. P. Garno, Phys. Rev. Lett. **41**, 1509 (1978).
- [29] T. Kubo and A. Gurevich, Phys. Rev. B **100**, 064522 (2019).
- [30] T. Kubo, Phys. Rev. Research **2**, 013302 (2020).
- [31] F. Herman and R. Hlubina, Phys. Rev. B **96**, 014509 (2017).
- [32] F. Herman, in *Proceedings of the 20th International Conference on RF Superconductivity* (2021) THPFDV010.
- [33] N. R. Groll, G. Ciovati, A. Grassellino, A. Romanenko, J. F. Zasadzinski, and T. Proslie, ArXiv:1805.06359.
- [34] While PCTS reports higher values of Γ/Δ_0 for both N-doped and EP samples than what is shown in Fig. 4, this is likely due to differences in the probing depth between the two techniques, as PCTS is more surface sensitive and probes regions with more pair-breaking mechanisms.
- [35] M. Barra, A. Cassinese, and R. Vaglio, Supercond. Sci. and Technol. **18**, 271 (2005).
- [36] C. Varmazis, J. R. Hook, D. J. Sandiford, and M. Strongin, Phys. Rev. B **11**, 3354 (1975).
- [37] P. Kostić, B. Veal, A. P. Paulikas, U. Welp, V. R. Todt, C. Gu, U. Geiser, J. M. Williams, K. D. Carlson, and R. A. Klemm, Phys. Rev. B **53**, 791 (1996).
- [38] V. G. Kogan and R. Prozorov, Phys. Rev. B **102**, 184514 (2020).

Supplemental Material for ‘The Anomalous Resonant Frequency Variation of Microwave Superconducting Niobium Cavities Near T_c ’

D. Bafia,^{1,*} A. Grassellino,¹ M. Checchin,¹ J. F. Zasadzinski,² and A. Romanenko¹

¹*Fermi National Accelerator Laboratory, Batavia, Illinois 60510, USA*

²*Department of Physics, Illinois Institute of Technology, Chicago, Illinois 60616, USA*

(Dated: January 6, 2022)

FREQUENCY VS TEMPERATURE FEATURES

Fig. 1 shows the five resonant frequency variations just below the critical transition temperature (T_c) in Nb SRF cavities. All five features have been observed while warming and cooling through T_c , which is expected as the superconducting phase transition is of the second order. The different features are characterized as follows. The “standard” feature shows a sharp transition of the resonant frequency to the normal conducting value. The “bump” feature, instead, shows a more gradual evolution of the frequency to the normal conducting value followed by a subsequent increase and decrease. A similar variation is observed for the “dip+bump” feature, but the resonant frequency shows a slight decrease before the subsequent behavior. A “foot” feature exhibits a frequency saturation before assuming the normal conducting value. Lastly, the “dip” feature shows a prominent decrease prior to full phase transition.

CAVITY PROCESSING TECHNIQUES

All the cavities used in this study first underwent bulk electropolishing to remove $\geq 120 \mu\text{m}$ of material. We used the five following final processing techniques to prepare the inner RF surface of our superconducting radio-frequency cavities:

- Electropolishing (EP): degas at 800°C in a vacuum better than 10^{-7} Torr for 3 hours followed by a $40 \mu\text{m}$ removal *via* electropolishing [1].
- Low temperature 120°C baking: degas at 800°C in vacuum for 3 hours followed by a $40 \mu\text{m}$ removal *via* EP. The cavity is then assembled for testing, evacuated, and baked *in-situ* at 120°C for 48 hrs [2].
- $75/120^\circ\text{C}$ baking: degas at 800°C in vacuum for 3 hours followed by a $40 \mu\text{m}$ removal *via* EP. The cavity is then assembled for testing, evacuated, and baked *in-situ* at 75°C for 4 hours followed by 120°C for 48 hrs [3, 4].
- Nitrogen infusion: after degassing at 800°C in vacuum for 3 hours, the temperature is lowered to 120°C and nitrogen at a partial pressure of

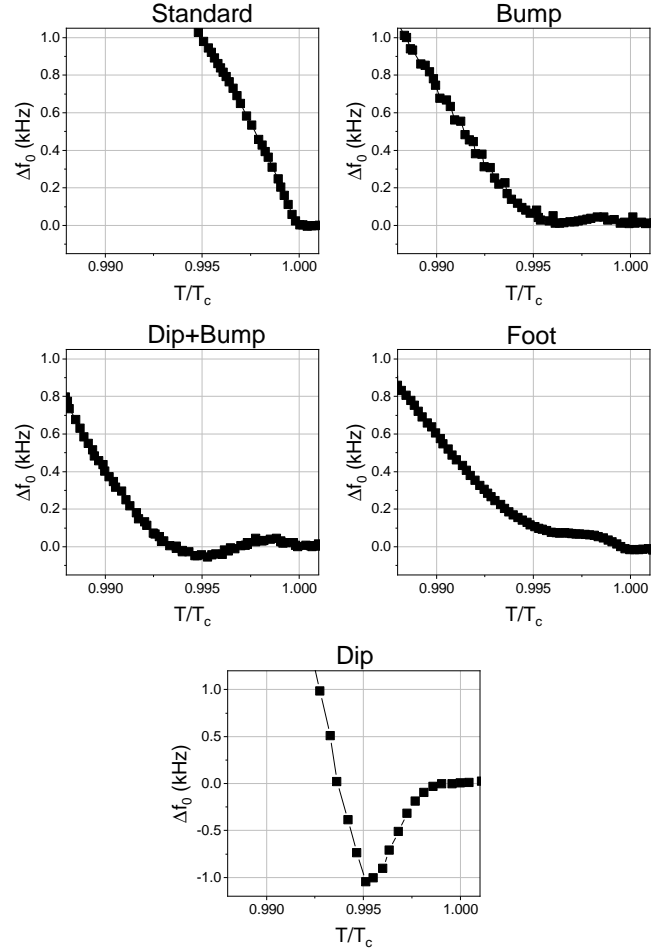


FIG. 1. Five observed resonant frequency variations of 1.3 GHz elliptical niobium SRF cavities near T_c .

~ 25 mTorr is introduced into the furnace. The cavity is then annealed at 120°C in this nitrogen atmosphere for 48 hours [5].

- Nitrogen doping: degas at 800°C in vacuum for 3 hours. While maintaining this temperature, nitrogen gas is injected at a partial pressure of 25 mTorr for a duration ranging from 1 to 20 minutes. The nitrogen supply is then cut off and vacuum is re-established, annealing the cavity further for 0-60 minutes. After the furnace run, the first few micrometers of the inner surface are removed by EP to eliminate the niobium nitride phase precipitates,

leaving nitrogen to exist as interstitial extending for several micrometers inside the material [6]. The nitrogen doping recipes are usually referred to as “x/y doping,” where x is the duration in minutes of the annealing stage with nitrogen and y is the post-nitrogen vacuum annealing duration. For example, “2/6 doping” means 2 minutes of annealing with 25 mTorr of nitrogen gas followed by 6 minutes with nitrogen pumped out.

EFFECT OF IMPURITY STRUCTURE ON FREQUENCY VARIATIONS NEAR T_c

A large ensemble of elliptical cavities was subjected to the treatments described in the previous section and tested using the methods laid out in the main text. The number of instances each feature in Fig. 1 occurred in resonant frequency shift data in the presence of a particular surface treatment was logged in Table I. We found that two of the electropolished cavities exhibited the standard feature while one showed the dip+bump feature. Both of the low temperature 120°C baked cavities exhibited the standard feature. The nitrogen infused cavities showed the foot, dip+bump, and standard features. The 75/120°C baked cavities revealed 4 out of the 5 behaviors near T_c , with the exception being the dip+bump. While a feature resembling a small dip was observed in one 75/120°C baked cavity, its magnitude of about 50 Hz was much smaller than what was observed for 22 doped cavities (~ 1 kHz). We believe this could have been a potential artifact of the helium pressure correction procedure. We note that 5 cavities exhibited a foot, suggesting that this behavior is characteristic of an oxygen enriched surface layer. All 22 nitrogen doped cavities investigated in this study exhibited a prominent dip in the resonant frequency.

	N-doped	N-Infused	75/120°C	120°C	EP
Dip	22		1 ^a		
Foot		1	5		
Bump			1		
Dip+Bump		2			1
Standard		1	3	2	2

^a $\Delta f_{dip} < 50$ Hz as compared to ~ 1 -2 kHz in doped cavities, likely an artifact of the pressure correction

TABLE I. Occurrence of features in $f_0(T)$ data near T_c for five typical SRF cavity surface treatments.

CALCULATING CONDUCTIVITY

Method

To calculate the complex conductivity, a method similar to the one laid out by Trunin was used [7]. The AC conductivity is given as

$$\sigma = \sigma_1 + i\sigma_2 = \omega\mu_0 \left(\frac{2R_s X_s}{(R_s^2 + X_s^2)^2} + i \frac{X_s^2 - R_s^2}{(R_s^2 + X_s^2)^2} \right), \quad (1)$$

where R_s and X_s are the surface resistance and reactance, respectively, and given by

$$R_s(T) = \frac{G}{Q_0(T)} \quad (2)$$

and

$$X_s(T) = -2G \frac{\Delta f_0(T)}{f_0} + X_n. \quad (3)$$

where $\Delta f_0(T)$ is the resonant frequency shift relative to the normal conducting value and f_0 is the resonant frequency. The parameter G denotes the geometry factor. For the elliptical 1.3 GHz cavities studied here, this factor is 270 Ω .

To obtain the additive constant X_n in Eq. 3, the normal conducting surface resistance measured just above the transition temperature $R_n(10 \text{ K})$ is required. In the local limit, valid for dirty Nb, $R_n(10 \text{ K}) = X_n(10 \text{ K})$ is true. However, when the local limit is not applicable, as is true for high purity niobium [2], the anomalous skin effect must be considered. The correct relationship between R_s and X_s is obtained using the universal impedance curves plotted against the dimensionless parameter α calculated by Reuter and Sondheimer in the microwave region [8]. The parameter α is proportional to $\ell^3/\rho\ell$, where ℓ is the mean free path, ρ is the resistivity, and $\rho\ell$ is a temperature independent material constant, which is $6 \times 10^{-16} \text{ } \Omega\text{m}^2$ for Nb [2]. Thus, by knowing ℓ , it is possible to obtain X_n , which in turn yields the total reactance.

Impedance Data

Fig. 2 shows the measured impedance data used to calculate the complex conductivities in Fig. 4 of the main text. Green circles and pink diamonds correspond to data acquired on EP and N-doped cavities, respectively. Data was acquired using methods laid out in [9]. Due to the change of signs in Eq. 3, a dip in frequency results in a peak in the reactance.

To ensure realistic values for the reactance, the experimental penetration depth at $T = 0 \text{ K}$ was calculated *via*

$$X_{s,0} = \omega\mu_0\lambda_{0,\text{exp}} \quad (4)$$

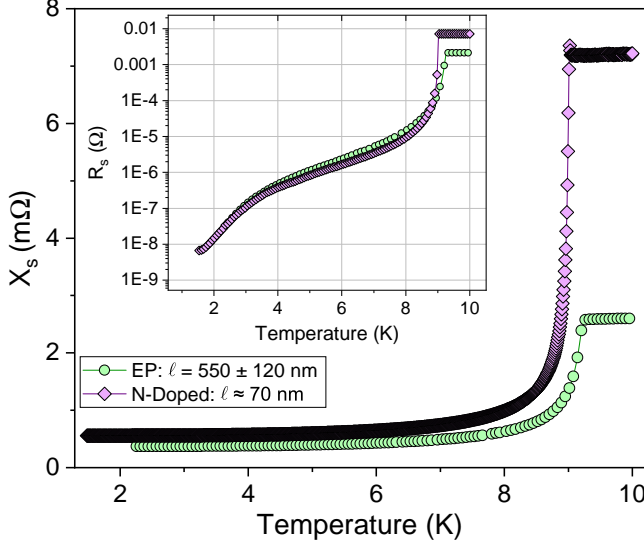


FIG. 2. Measured surface resistance and surface reactance of two 1.3 GHz cavities treated to either electropolishing (EP) or N-doping.

and compared with the effective penetration depth obtained from

$$\lambda_0 = \lambda_L \sqrt{1 + \frac{\xi_0}{\ell}}. \quad (5)$$

For Nb, $\lambda_L = 39$ nm and $\xi_0 = 38$ nm [10]. The experimental and calculated results shown in Table II are in good agreement.

Treatment	$X_{s,0}$ [Ω]	ℓ [nm]	$\lambda_{0,\text{exp}}$ [nm]	λ_0 [nm]
EP	3.70×10^{-4}	550	36 ± 8	40
N-Doped	5.58×10^{-4}	70	54 ± 2	48

TABLE II. Comparison of experimentally and theoretically obtained values for the penetration depth at $T = 0$ K.

Modeling the Complex Conductivity

The non-monotonic dependence of the real part of the complex conductivity in BCS superconductors [11, 12], called the coherence peak, arises due to the singularity in the superconducting density of states at the gap edge. According to Dynes [13], inelastic scattering smears the singularity and introduces subgap quasiparticle states according to

$$\frac{N}{N_0} = \frac{E + i\Gamma}{\sqrt{(E + i\Gamma)^2 - \Delta^2}}, \quad (6)$$

where Γ is a phenomenological smearing parameter. By incorporating such a phenomenological model into the

conductivity, it is possible to obtain a measure of pair-breaking processes present in a system from the height and width of the coherence peak.

To extract the level of inelastic scattering from the SRF cavity conductivity data presented in Fig. 4 of the main text, we used a slightly modified version of the Mattis-Bardeen conductivity [12] with the Dynes smearing parameter Γ [13] built in

$$\frac{\sigma_1}{\sigma_n} = \frac{2}{\hbar\omega} \int_{\Delta}^{\infty} \frac{[f(E) - f(E + \hbar\omega)]g(E, \Gamma)}{\sqrt{(E + i\Gamma)^2 - \Delta^2}} dE + \frac{1}{\hbar\omega} \int_{\Delta - \hbar\omega}^{-\Delta} \frac{[1 - 2f(E + \hbar\omega)]g(E, \Gamma)}{\sqrt{(E + i\Gamma)^2 - \Delta^2}} dE, \quad (7)$$

$$\frac{\sigma_2}{\sigma_n} = \frac{2}{\hbar\omega} \int_{\Delta - \hbar\omega, -\Delta}^{\Delta} \frac{[1 - 2f(E + \hbar\omega)]g(E, \Gamma)}{\sqrt{(\Delta^2 - (E + i\Gamma)^2)}} dE, \quad (8)$$

$$g(E, \Gamma) = \frac{(E + i\Gamma)((E + i\Gamma) + \hbar\omega) + \Delta^2}{\sqrt{((E + i\Gamma) + \hbar\omega)^2 - \Delta^2}}. \quad (9)$$

* dbafia@fnal.gov

- [1] H. Padamsee, J. Knobloch, and T. Hays, *RF Superconductivity for Accelerators* (Wiley-VCH Verlag GmbH and Co., KGaA, Weinheim, 1998).
- [2] H. Padamsee, *RF Superconductivity: Volume II: Science, Technology and Applications* (Wiley-VCH Verlag GmbH and Co., KGaA, Weinheim, 2009).
- [3] A. Grassellino, A. Romanenko, D. Bice, O. Melnychuk, A. C. Crawford, S. Chandrasekaran, Z. Sung, D. A. Sergatskov, M. Checchin, S. Posen, M. Martinello, and G. Wu, ArXiv:1806.09824.
- [4] D. Bafia, A. Grassellino, O. Melnychuk, A. Romanenko, Z.-H. Sung, and J. Zasadzinski, in *Proceedings of the 19th International Conference on RF Superconductivity* (HZDR, Dresden, Germany, 2019) p. 586.
- [5] A. Grassellino, A. Romanenko, Y. Trenikhina, M. Checchin, M. Martinello, O. S. Melnychuk, S. Chandrasekaran, D. A. Sergatskov, S. Posen, A. C. Crawford, S. Aderhold, and D. Bice, *Supercond. Sci. Technol.* **30**, 094004 (2017).
- [6] A. Grassellino, A. Romanenko, D. Sergatskov, O. Melnychuk, Y. Trenikhina, A. Crawford, A. Rowe, M. Wong, T. Khabiboulline, and F. Barkov, *Supercond. Sci. and Technol.* **26**, 102001 (2013).
- [7] M. R. Trunin, A. A. Zhukov, and A. T. Sokolov, *Zh. Eksp. Teor. Fiz.* **111**, 696 (1997).
- [8] G. E. H. Reuter and E. H. Sondheimer, *Proc. Roy. Soc. London Ser. A* **195**, 336 (1948).
- [9] D. Bafia, Ph.D. thesis, Illinois Institute of Technology (2020).
- [10] B. W. Maxfield and W. L. McLean, *Phys. Rev.* **139**, A1515 (1965).
- [11] J. Bardeen, L. N. Cooper, and J. R. Schrieffer, *Phys. Rev.* **108**, 1175 (1957).
- [12] D. C. Mattis and J. Bardeen, *Phys. Rev.* **111**, 412 (1958).
- [13] R. C. Dynes, V. Narayanamurti, and J. P. Garno, *Phys. Rev. Lett.* **41**, 1509 (1978).